

# Interphase effects in dental nanocomposites investigated by small-angle neutron scattering

Kristen S. Wilson,<sup>1,\*</sup> Andrew J. Allen,<sup>2</sup> Newell R. Washburn,<sup>1,3,4</sup> Joseph M. Antonucci<sup>1</sup>

<sup>1</sup>Polymers Division, National Institute of Standards and Technology, Gaithersburg, Maryland 20899

<sup>2</sup>Ceramics Division, National Institute of Standards and Technology, Gaithersburg, Maryland 20899

<sup>3</sup>Department of Chemistry, Carnegie Mellon University, Pittsburgh, Pennsylvania 15213

<sup>4</sup>Department of Biomedical Engineering, Carnegie Mellon University, Pittsburgh, Pennsylvania 15213

Received 25 January 2006; revised 9 June 2006; accepted 22 June 2006

Published online 16 November 2006 in Wiley InterScience (www.interscience.wiley.com). DOI: 10.1002/jbm.a.30975

**Abstract:** Small-angle and ultrasmall-angle neutron scattering (SANS and USANS) were used to characterize silica nanoparticle dispersion morphologies and the interphase in thermoset dimethacrylate polymer nanocomposites. Silica nanoparticle fillers were silanized with varying mass ratios of 3-methacryloxypropyltrimethoxysilane (MPTMS), a silane that interacts with the matrix through covalent and H-bonding, and *n*-octyltrimethoxysilane (OTMS), a silane that interacts through weak dispersion forces. Interphases with high OTMS mass fractions were found to be fractally rough with fractal dimensions,  $D_s$ , between 2.19 and 2.49. This roughness was associated with poor interfacial adhesion and inferior mechanical properties. Mean interparticle distances calculated for composites containing 10 mass % and 25 mass % silica suggest that the nanoparticles treated with more

MPTMS than OTMS may be better dispersed than OTMS-rich nanoparticles. The results indicate that the covalent bonding and H-bonding of MPTMS-rich nanoparticles with the matrix are necessary for preparing well-dispersed nanocomposites. In addition, interphases containing equal masses of MPTMS and OTMS may yield composites with overall optimal properties. Finally, the combined SANS/USANS data could distinguish the differences, as a function of silane chemistry, in the nanoparticle/silane and silane/matrix interfaces that affect the overall mechanical properties of the composites. © 2006 Wiley Periodicals, Inc. *J Biomed Mater Res* 81A: 113–123, 2007

**Key words:** aggregation; dispersion; nanoparticle; silane; silica; thermoset composite

## INTRODUCTION

The dimethacrylate-based composites used as dental restoratives<sup>1,2</sup> require improvements<sup>3–7</sup> that may be addressed by the use of silica nanoparticle fillers. However, due to their high mobility and surface-to-volume ratios, nanoparticles often form microscopic aggregates during processing, thus offsetting the potential benefits of their nanoscopic dimensions. In general, a compatibilizing organic coating improves nanoparticle dispersion in a matrix.<sup>8</sup> In dental com-

posites, the silica filler is often surface-treated with 3-methacryloxypropyltrimethoxysilane (MPTMS) to deter particle aggregation and promote interfacial adhesion by allowing the particle surfaces to copolymerize with the polymer matrix. By contrast, *n*-octyltrimethoxysilane (OTMS), a non-reactive aliphatic silane, does not react with the resin matrix but interacts mainly through weak van der Waals forces. Dual-silanization of silica particles with blends of reactive MPTMS and non-reactive OTMS offers a number of potential advantages compared to silanization with MPTMS only. These advantages include improved uncured paste handling characteristics, higher double-bond conversion during photopolymerization,<sup>9</sup> improved durability in the aqueous oral environment, and lower polymerization stress.<sup>10</sup>

The aim of this research was to relate the chemical composition of the silane-derived interphase to mechanical properties, mesoscopic nanoparticle morphologies, and nanoscale interphase structures in model dental nanocomposites. The chosen system was a reasonable model for a microfilled composite

\*Present address: Bayer MaterialScience LLC, Pittsburgh, PA 15205, USA.

Correspondence to: A. J. Allen; e-mail: andrew.allen@nist.gov

Contract grant sponsor: NIST with the National Institute of Dental and Craniofacial Research; contract grant number: Y1-DE-1021-04

because these types of dental restoratives typically contain 20%–45% by volume (35%–60% by mass) silica nanoparticles, 10–120 nm in diameter.<sup>11,12</sup> A series of fillers were prepared with varying ratios of MPTMS and OTMS surface chemistries. Composites with four different concentrations of silanized silica fillers were prepared, and the changes in composite morphology over a large size range (1 nm–10  $\mu$ m) were studied using combined small-angle neutron scattering (SANS) and ultrasmall-angle neutron scattering (USANS) studies. Although there have been other studies of silica nanocomposites by SANS,<sup>13</sup> this technique has not been rigorously explored previously as a tool in dental composites research.

## EXPERIMENTAL SECTION\*

### Materials

The matrix of the composites was comprised of a 50:50 by mass mixture of 2,2-bis[*p*-(2'-hydroxy-3'-methacryloxypropoxy)-phenyl] propane (BisGMA) and triethylene glycol dimethacrylate (TEGDMA) (Esstech, Essington, PA) activated for photopolymerization with an initiator system of ethyl 4-dimethylaminobenzoate (4E) and camphorquinone (CQ) (Aldrich, Milwaukee, WI), at mass fractions of 0.8 and 0.2%, respectively. Aerosil OX50 fumed amorphous silica (Degussa, Dublin, OH) was silanized with MPTMS and OTMS (Gelest, Tullytown, PA). The particles ranged from 10 to 80 nm in diameter with a primary particle size of 40 nm according to the manufacturer. Silanizations were conducted in cyclohexane (J.T. Baker, Phillipsburg, NJ) using *n*-propylamine<sup>14</sup> as a catalyst (Aldrich, Milwaukee, WI).

### Silanization of silica nanoparticles

The nanoparticles were treated with silanes (10% by mass relative to silica) using a previously reported procedure.<sup>14</sup> The mass ratios of MPTMS:OTMS charged to the silanization reactions were varied from 1:0, 0.75:0.25, 0.5:0.5, 0.25:0.75, and 0:1. In a representative procedure, the silica powder (5.0  $\pm$  0.05 g), cyclohexane (100 mL), *n*-propylamine (0.1  $\pm$  0.01 g), and MPTMS (0.55  $\pm$  0.01 g) were agitated in a round bottom flask at 25°C  $\pm$  5°C for 30 min and then at 60°C  $\pm$  5°C for 30 min. The mixture was placed under vacuum ( $\approx$ 2.7 kPa) using a rotary evaporator at 60°C  $\pm$  5°C for approximately 15 min. The resulting powder was then heated at 95°C  $\pm$  5°C for 1 h under the same vacuum in the rotary evaporator and then at 80°C for 18 h in a vacuum oven ( $\approx$ 2.7 kPa).

\*Certain commercial materials and equipment are identified in this report only to specify adequately the experimental procedure. In no case does such identification imply recommendation by NIST nor does it imply that the material or equipment identified is necessarily the best available for this purpose.

### Composite preparation for SANS studies and mechanical testing

For the SANS studies, the silanized silica powders (10, 25, 45, and 60% by mass; 5.9, 15.8, 31.5, and 45.7% by volume, respectively, calculated based on the density of silica) were thoroughly mixed into the photo-activated resin until the composite pastes appeared homogeneous and semi-transparent. The pastes ( $\approx$ 0.15 g) were photopolymerized between two sheets of Mylar film pressed between glass slides for 1 min per side using a Dentsply Triad 2000 visible light curing system (York, PA;  $\lambda$  = 470 nm). For mechanical testing, 60% by mass of the silanized silica powders were mixed into the resin as described previously. The composite pastes were then pressed into circular molds (for biaxial flexure strength, BFS) or rectangular molds (for three point bend), photo-cured for 1 min per side between Mylar film and glass slides, and stored in distilled water at 37°C  $\pm$  0.5°C for 24 h prior to mechanical testing according to procedures established in the literature.<sup>15</sup>

### Characterization of physical and mechanical properties

The silanized silica nanoparticles were analyzed for mass loss on heating using a TA Instruments Q500 thermogravimetric analyzer (TGA). The particles (0.20  $\pm$  0.02 mg) were heated to 600°C under air or ultra-pure nitrogen at 10°C per min.

Three-point bend and BFS tests were conducted at a cross-head speed of 0.5 mm min<sup>-1</sup> using a Universal Testing Machine model 5500R (Instron, Canton, MA). The three-point bend test utilized a 20 mm span. The moduli and strength values reported were the average of 5–7 specimens from which the standard deviation uncertainties were deduced.

Scanning electron microscopy (SEM) images of the composite were obtained using a field emission SEM (FE-SEM, Hitachi 4700) operating at 1 kV. The composites were embedded in epoxy and cut with an Allied diamond wafering blade. The surfaces were sanded with silicon carbide sandpaper down to 4000 grit and then polished with diamond-sprayed polishing cloths. The surfaces were then etched for 10 min in a quartz-barrel plasma cleaner (model SP100, Anatech, Alexandria, VA) to expose the silica nanoparticles.

Bright-field transmission electron micrographs were obtained with a Philips EM400T transmission electron microscope at an accelerating voltage of 120 kV. Sections approximately 70 nm thick were cut from polymerized nanocomposites at room temperature using a Leica ultramicrotome equipped with a diamond knife. These sections were collected on the surface of a water-filled trough and retrieved using 200 mesh copper grids.

### Microstructure characterization by SANS and USANS

SANS measurements were carried out using the NIST/ExxonMobil/University of Minnesota NG7 SANS instrument<sup>16</sup> at the NIST Center for Neutron Research (NCNR), Gaithersburg, MD. USANS measurements were made

using the BT5 NSF USANS facility<sup>17</sup> at NCNR. For SANS, the neutron wavelength,  $\lambda$ , was 0.8 nm and four different instrument configurations were used, with the data recorded on a 2D detector. Data were corrected for detector sensitivity, electronic and parasitic background effects, and sample absorption, then calibrated against the incident beam flux and normalized to unit sample volume. Finally, the SANS data were circularly-averaged to give the absolute scattering cross-section intensity as a function of  $q$  [where  $q = (4\pi/\lambda) \sin(\phi_S/2)$  where  $\phi_S$  is the scattering angle] in the range  $0.005 \text{ \AA}^{-1} < q < 0.2 \text{ \AA}^{-1}$ . The USANS instrument employs Bonse-Hart Si (220) crystal diffraction optics with  $\lambda = 0.24 \text{ nm}$  to extend the minimum  $q$  down to  $0.00003 \text{ \AA}^{-1}$ . The data were corrected for the empty beam (blank) subtraction, calibrated with respect to the incident beam, and de-smearred to remove slit-smearing effects. The combined SANS/USANS data were intercalated and normalized with respect to each other in order to produce, in each case, a single data set of the scattering cross-section ( $d\Sigma/d\Omega$ , or  $I\{q\}$ ) versus  $q$ .

The combined data were analyzed using a combination of four theoretical models for various parts of the composite microstructure. At  $q > 0.02 \text{ \AA}^{-1}$ , the  $q^{-4}$  Porod scattering law<sup>18</sup> was assumed in order to determine the total silica/matrix interfacial surface area,  $S_T$ , from:

$$\frac{d\Sigma}{d\Omega} = \frac{2\pi|\Delta\rho|^2 S_T}{q^4} + \text{BGD} \quad (1)$$

where  $|\Delta\rho|^2$  is the scattering contrast between silica and the polymer matrix ( $|\Delta\rho|^2 = 4.414 \times 10^{28} \text{ m}^{-4}$ ) and BGD is the incoherent flat background scattering. The presence of the silane interphase complicates the assumption of a 2-phase system composed of silica particles within a polymer matrix. However, the interphase thickness is assumed to be much smaller than the silica particle size; thus a two-phase model can be applied for most purposes.

Close inspection of the scattering data for some of the samples revealed that the terminal exponent in  $q$  was actually slightly  $<4$  (see below), indicating the presence of a self-affine surface-fractal structure surrounding the silica particles. This structure masks any effect of a diffuse interface caused by a gradation in the silane concentration across the thickness of the interphase region, which could have given steeper than  $q^{-4}$  scattering. The fractal structure was modeled by fitting the data with a surface-fractal function<sup>19</sup> for  $q > 0.01 \text{ \AA}^{-1}$ :

$$\frac{d\Sigma}{d\Omega} = \frac{\pi \xi_S^4 |\Delta\rho|^2 S_0 \Gamma(5 - D_S) \sin[(3 - D_S) \arctan(q\xi_S)]}{[1 + (q\xi_S)^2]^{(5-D_S)/2} q \xi_S} + \text{BGD} \quad (2)$$

where  $S_0$  is the smooth surface area measured for a scale dimension  $>$  the correlation length,  $\xi_S$ ,  $D_S$  is the surface-fractal exponent, and  $\Gamma(x)$  denotes the mathematical gamma function. For  $q\xi_S \gg 1$ ,  $d\Sigma/d\Omega \sim q^{(6-D_S)}$ , which gives Porod  $q^{-4}$  scattering if  $D_S = 2$ . Also, the surface area measured for a roughness dimension,  $r$ , is given by  $S(r) = S_0 (\xi_S/r)^{(D_S-2)}$  and the maximally-rough surface area is given for the minimum roughness dimension,  $r = r_C$ . The model fit gives  $S_0$ ,  $D_S$ , and  $\xi_S$ . If the maximally-rough surface area is assumed to equal  $S_T$ , from the Porod scattering, comparison of  $S_0$  and  $S_T$  can be used to esti-

mate  $r_C$ . However, our main purpose was to determine the degree to which  $D_S$  varied from two as a function of the silica particle concentration and the MPTMS/OTMS interphase composition.

The combined SANS/USANS data were also fitted over all  $q$  using a two- or three-component lognormal volume fraction size distribution model to calculate the scattering from the silica particles within the polymer matrix<sup>19,20</sup>:

$$\frac{d\Sigma}{d\Omega_i} = |\Delta\rho|^2 \left\{ \int \Phi_i(D) F_i^2(q) V_i(D) dD \right\} P(q) \quad (3)$$

where the form factor used,  $F_i^2(q)$ , is that for a spheroid of near-globular aspect ratio,  $\beta = 1.2$ ,  $V_i(D)$  is the particle volume for diameter,  $D$ , i.e.,  $V_i(D) = \beta\pi D^3/6$ , the cross-section is averaged over the  $i$ -component size distribution,  $\Phi_i(D)$ , and  $P(q)$  is the structure factor for particle-particle interactions discussed below. Since the silica particles are not exact spheres, the aspect ratio,  $\beta$ , was set to 1.2, rather than 1.0, to allow for some dispersion in shape and orientation within the defined lognormal size distributions. For each component,  $\Phi(D)$  is given by:

$$\Phi(D) = \frac{\Phi_T}{[2\pi \ln(D_{\text{MEDIAN}}/D_{\text{MODE}})]^{1/2}} \left( \frac{1}{D} \right) \times \exp \left\{ -\frac{[\ln(D/D_{\text{MEDIAN}})]^2}{2 \ln(D_{\text{MEDIAN}}/D_{\text{MODE}})} \right\} \quad (4)$$

where the total volume fraction,  $\Phi_T$ , the mode diameter,  $D_{\text{MODE}}$ , and the distribution width were fitted for each component. However, the median diameter,  $D_{\text{MEDIAN}}$ , and the mean diameter,  $D_{\text{MEAN}} = (D_{\text{MEDIAN}}^{3/2})/(D_{\text{MODE}}^{1/2})$ , are the derived parameters that, together with  $D_{\text{MODE}}$  and  $\Phi_T$  are most useful to describe each lognormal distribution.

Interparticle interference effects were taken into account for the primary lognormal size distribution of silica nanoparticles. In the present case, only a very approximate attempt was made to parameterize the interference effects through a functional form of  $P(q)$ :

$$P(q) = \{1 - \nu F_{\text{SPH}}^2(q, D_{\text{INT}})\} \quad (5)$$

where  $\nu$  is the local coordination number for nearest-neighbor particles and  $F_{\text{SPH}}^2(q, D_{\text{INT}})$  is effectively a form-factor function for spheres with radius,  $D_{\text{INT}}$ , where  $D_{\text{INT}}$  is the mean nearest-neighbor distance, averaged over the particle size distribution.

Finally, as a check on the absolute volume fraction of silica present, the scattering invariant,  $Q_{\text{INVARIANT}}$ ,<sup>18</sup> was calculated for a selection of the combined SANS/USANS data sets:

$$Q_{\text{INVARIANT}} = 2\pi^2 \Phi_T (1 - \Phi_T) |\Delta\rho|^2 = \int_0^\infty Q^2 \frac{d\Sigma}{d\Omega}(Q) dQ \quad (6)$$

where  $\Phi_T$  is now the total volume fraction of silica (all components) and the integral is taken over the entire SANS/USANS data set after subtraction of the BGD term at high  $q$ .

The uncertainty in the TGA mass % data was  $\pm 0.2$  mass %. The uncertainty in the  $I(q)$  data from neutron scattering was  $\pm 1\%$ . Indicated uncertainties are one estimated standard deviation.

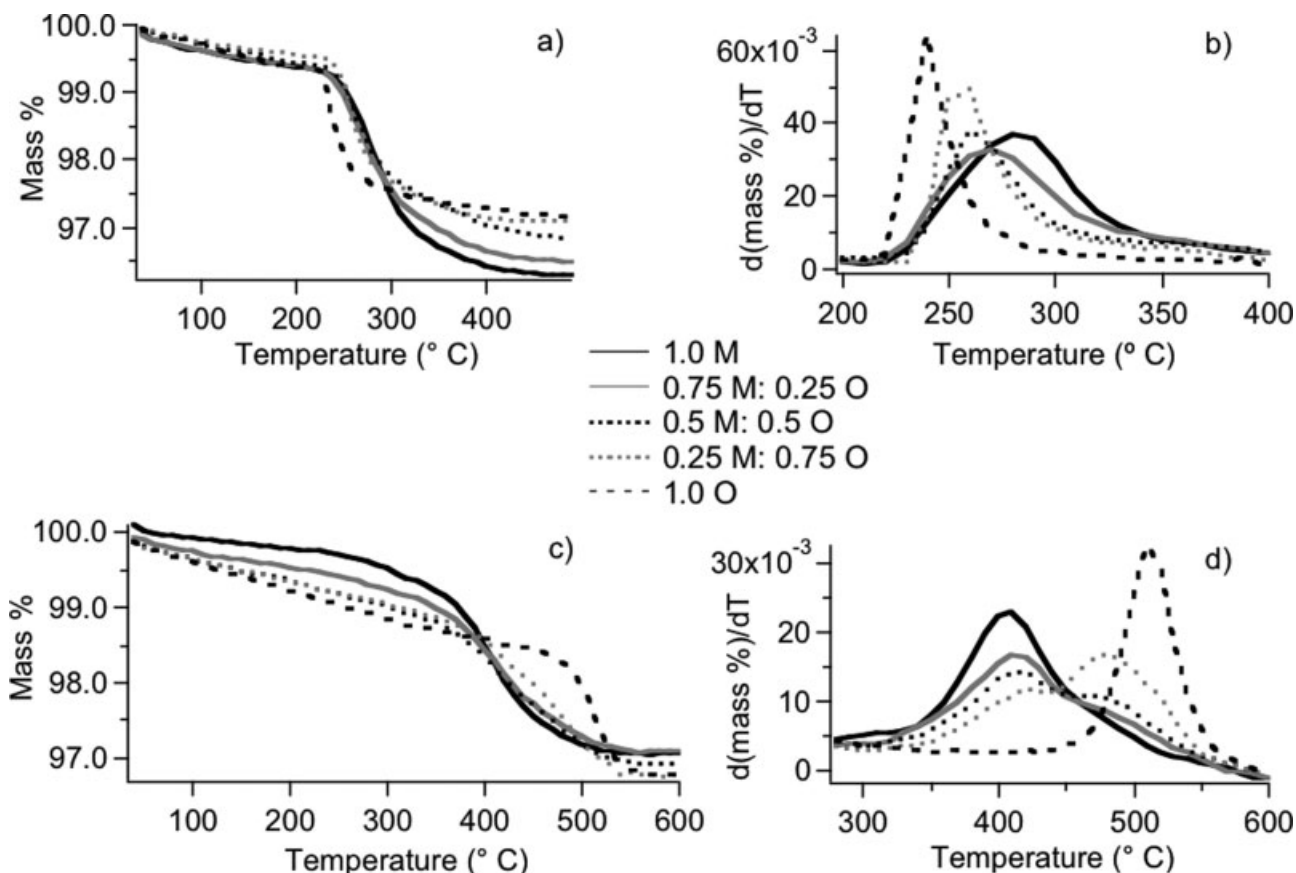


**Figure 1.** Mass loss with respect to temperature by thermogravimetric analysis of the silanized silica nanoparticles with varying ratios of MPTMS and OTMS (a) in air, (b) derivative of a, (c) in ultra-pure nitrogen, and (d) derivative of c.

## RESULTS AND DISCUSSION

### Thermal characterization of silanized silica nanoparticles

TGA was used to verify that the silica nanoparticles have controlled silane surface chemistries (Fig. 1). The data compare mass loss due to thermal degradation of the silanes for each type of silanized silica. The final mass losses in air ( $3.24\% \pm 0.38\%$ ) are comparable to those in nitrogen ( $3.09\% \pm 0.16\%$ ). In air, as the silane agent is changed from MPTMS to OTMS, the temperature of the mass loss inflection point decreases in a stepwise manner and the sharpness of the transition increases. In nitrogen, a very different change is observed. The MPTMS inflection point occurs at  $\approx 400^\circ\text{C}$ , the blended silanes display two inflection points, and the OTMS inflection point is at  $\approx 510^\circ\text{C}$  ( $270^\circ$  higher than in air). In the absence of oxygen, the thermal degradations are inhibited and occur at higher temperatures. This effect is more exaggerated for OTMS than for MPTMS, possibly because MPTMS contains oxygen in its methacrylate group and the degradation may be partially self-cat-

alyzed. The silyl ether oxygens are not likely to promote degradation since they are tightly held within condensed silica networks.

### Characterization of nanocomposite mechanical properties

The mechanical properties of the composites containing 60% mass fraction silanized silica (60%  $\text{SiO}_2$  composites) have been described in detail elsewhere<sup>9</sup> and are summarized here in Figure 2. The BFS and three-point bend flexure strengths are comparable for the three composites containing the highest fractions of MPTMS in the interphase. The BFS of the composite with the 0.5:0.5 MPTMS:OTMS mass ratio (0.5 M:0.5 O composite) is significantly greater than for all the other composites ( $p \leq 0.05$ ) except the 1.0 M composite. With increased OTMS fractions in the interphase (0.25 M:0.75 O and 1.0 O), the flexure strengths and BFS values of the composites decrease. A similar trend is seen in the moduli of the composites, with the OTMS composite having the lowest modulus.

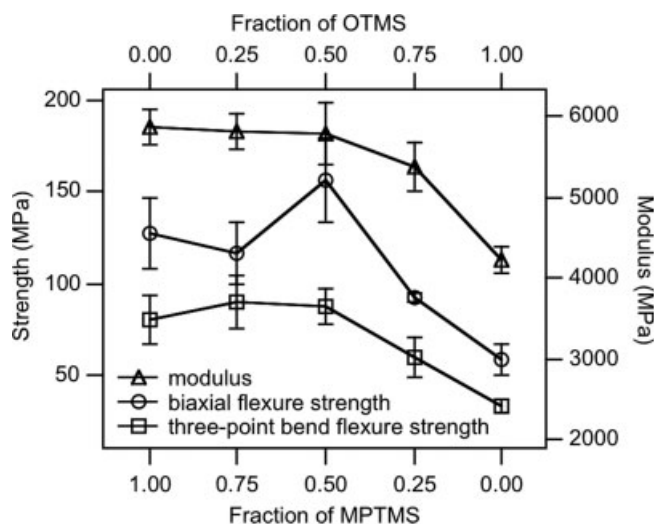


**Figure 2.** Moduli (right axis), biaxial flexure strengths, and three-point bend flexure strengths (left axis) of 60% SiO<sub>2</sub> composites with varied silane interphase compositions. Lines are drawn to guide the eye.

### Effect of silane composition on nanoscale interphase structure

To assess more accurately the influence of the different interphase compositions on the mechanical properties of the nanocomposites, we analyzed a series of composites with SANS and USANS. For modeling the data, we assumed two phases (silica and polymer matrix) with distinct scattering length densities. The silane interphase was assumed to have a scattering length density intermediate between the silica and the polymer matrix and for simplicity was not modeled in this study. For the highest silica particle loadings (60% mass and, to some extent, 45% mass) the silane content was sufficient to reduce the effective scattering contrast between the particles and the average (silane/polymer) matrix so that the model results accounted for less than the total silica present. However, this did not affect the morphology issues discussed below.

In the four silica composite concentrations investigated, deviations from  $q^{-4}$  behavior in the Porod region of the scattering profile are observed as the interphase chemistry is gradually changed from 1.0 M to 1.0 O (Fig. 3). The slope of the scattering curve decreases as the fraction of OTMS in the interphase is increased. This effect becomes more apparent as the mass fraction of silanized silica in the composite is increased. To interpret, quantitatively, the effects in the high  $q$  region, the scattering data were fit with a surface-fractal model function (2).

The fractal model results correlate with a slight increase in the Porod surface area,  $S_T$ , as the OTMS fraction increases (Fig. 4). This subtle trend is consistent in the composites at all four silica concentra-

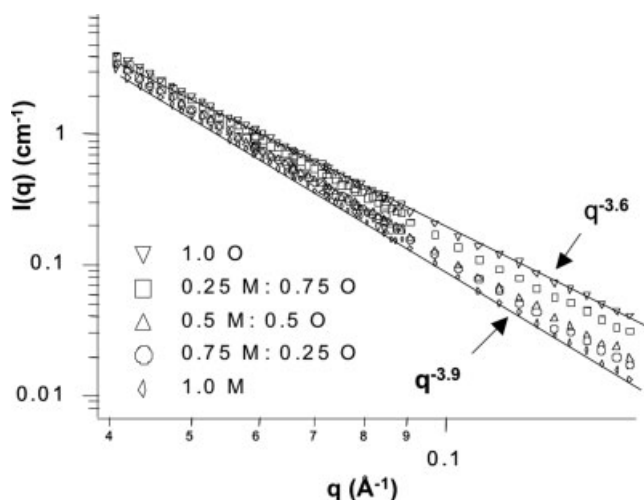


**Figure 3.**  $I(q)$  versus  $q$  expanded in the high  $q$  regime for 60% SiO<sub>2</sub> composites with varying interphase compositions. Deviation from  $q^{-4}$  as the fraction of MPTMS decreases and OTMS increases suggests surface fractal behavior at the interphase. Exponents fit uncertainty  $< \pm 0.05$ . The lines indicate the range of exponents found.

tions, and suggests that rough interfaces exist in the OTMS-rich composites that do not exist in the MPTMS-rich composites. In addition, the fractal model fit also provides the surface fractal exponent,  $D_s$ , for each composite (Fig. 5), where  $D_s = 2$  describes smooth interfaces and  $D_s > 2$  describes fractally rough interfaces. In Figure 5, it is clearly seen that  $D_s$  is very close to 2 for the 1.0 M, 0.75 M: 0.25 O, and 0.5 M: 0.5 O composites and then sharply increases to 2.2 and 2.5 for the 0.25 M: 0.75 O and 1.0

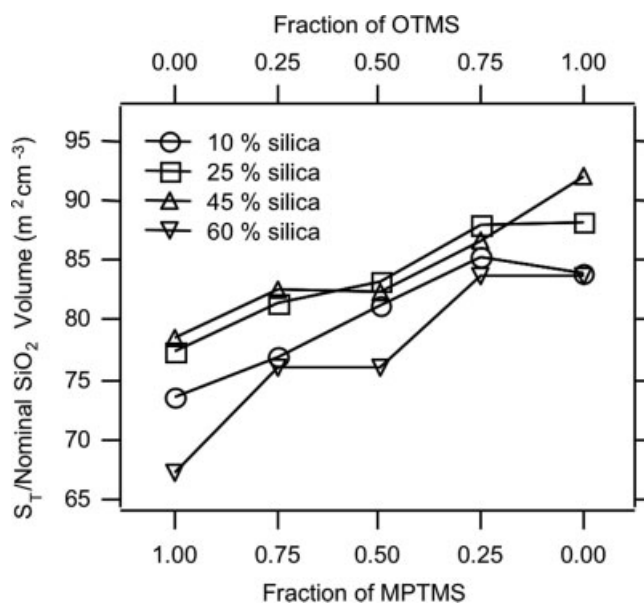


**Figure 4.** Total surface areas normalized with respect to nominal silica volume deduced from Porod scattering fits to the high  $q$  data.

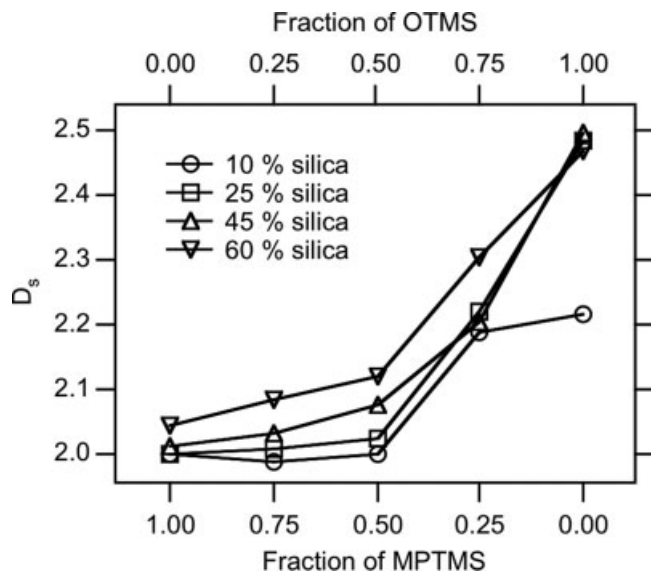


**Figure 5.** Surface fractal exponents ( $D_s$ ) as a function of interphase chemistry for the four silica composite concentrations investigated in this study.

O composites, respectively. Thus, fractally rough interfaces exist in the composites containing the highest OTMS mass fraction.

The relative fractal roughness detected in the composites with various interphase chemistries provides insights into the nature of the adhesive or non-adhesive qualities of the silanes. The silane interphases interact with the surrounding polymer matrix phase through covalent bonding, H-bonding, van der Waals interactions, or some combination thereof. For the 1.0 M composite, the  $S_T$  and  $D_s$  values indicate smooth interfaces within the composite. It is inferred that the Porod scattering intensity originates primar-

ily from the smooth nanoparticle/silane network interface. An interface between the silane network and the polymer matrix is not detected. Therefore, the 1.0 M interphase mixes and reacts with the matrix sufficiently to render it indistinguishable from the matrix. This scattering characteristic is maintained for the 1.0 M, 0.75 M:0.25 O, and 0.5 M:0.5 O composites, indicating that significant interphase/matrix copolymerization and H-bonding interactions occur even when up to half of the interphase is OTMS, providing significant particle/matrix adhesion.

For the 0.25 M: 0.75 O and 1.0 O composites, however, two interfaces exist: a smooth nanoparticle/silane network interface and a fractally rough silane network/polymer matrix interface. The rough, fractal-like interface is detected because of poor bonding between the OTMS-rich interphase and the polymer matrix phase. These interfaces cause the shallow slope in the Porod regime and a value of  $D_s > 2$  (Fig. 6). Such effects are indicative of poor adhesion and poor OTMS/polymer matrix compatibility.

#### Effect of filler concentration on composite morphology

Nanoparticle microstructures within the composites were investigated as a function of filler concentration. The volume weighted particle size distribution,  $V(D)$ , derived from the model fitting, changes appreciably as a function of filler concentration. The ratio  $V(D)/V(D)_{\max}$  vs. diameter curves narrow and shift to smaller diameters as the concentration of silanized silica increases from 10 and 25% to 45 and 60%  $\text{SiO}_2$  (Fig. 7). Since the same batch of silica was used for all the composites, the particle size differen-

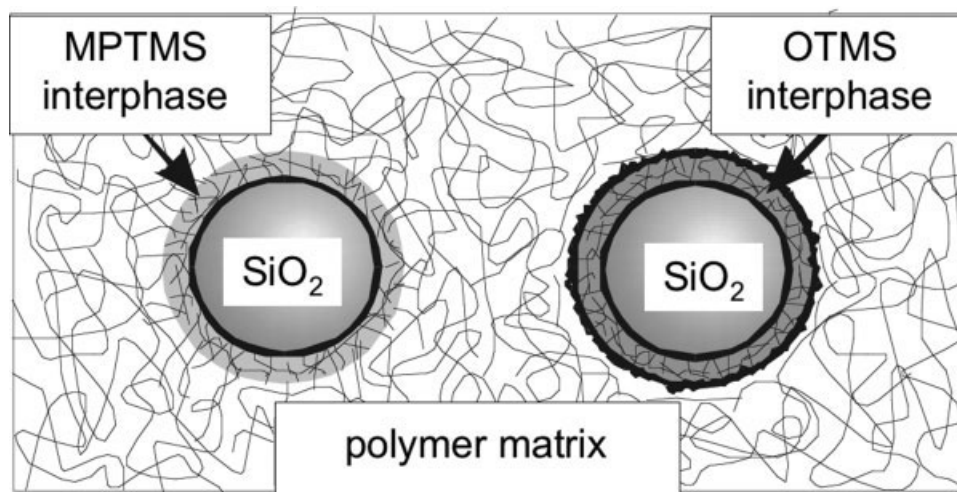


**Figure 6.** A diagram showing the differences between the MPTMS and OTMS interphases. There is a distinct rough interface between OTMS and the polymer matrix whereas the MPTMS interphase is copolymerized with the matrix so that the MPTMS-matrix interface is indistinguishable. In this diagram, the sizes of the interphase regions have been exaggerated relative to the size of the silica nanoparticles.

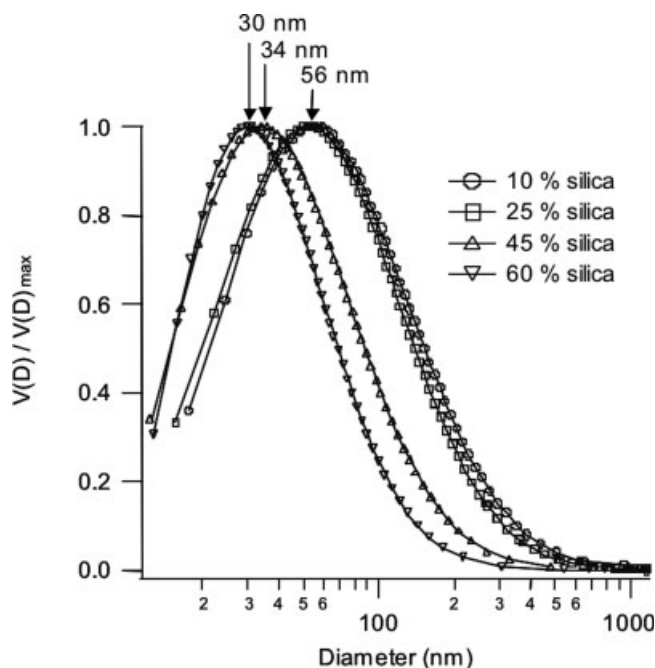


**Figure 7.** Volume weighted size distributions normalized with respect to maximum volume,  $V(D)_{\max}$ , for composites containing four concentrations of 1.0 O silica.

ces are caused by the differences in nanoparticle microstructure.

In the 45 and 60%  $\text{SiO}_2$  composites, as observed in SEM (Fig. 8), the spatial arrangement of the particles is nearly close-packed and the overall distribution is relatively homogeneous. In the 45%  $\text{SiO}_2$  composites, there are some regions of polymer-rich voids. The maxima in  $V(D)/V(D)_{\max}$  (Fig. 7) are located at 30 and 34 nm for the 60 and 45%  $\text{SiO}_2$  composites, respectively. These mean diameters are acceptably close to the manufacturer's nominal primary particle size of 40 nm derived from SEM. The results indicate that the SANS data are dominated by scattering from individual particles, not from particle clusters. Examination of the scattering profiles in Figure 9 reveals a distinct flattening of the scattering data for the 60%  $\text{SiO}_2$  composites at low  $q$ . This flattening or "topping out" of the scattered intensity at low  $q$  indicates that if any aggregates are present, then they are too large to scatter in the measured  $q$  range. For the 10, 25, and 45%  $\text{SiO}_2$  composites, the scattering continues to increase in intensity with decreasing  $q$  at the lowest  $q$  values, which indicates scattering both from individual particles and particle aggregates. For the 45%  $\text{SiO}_2$  composite, the aggregate volume fraction measured by model fitting is very small ( $\approx 0.5\%$  by volume) compared to the total silica volume fraction in the composite. Individual particles, particle clusters, and polymer-rich regions are observed in the 10 and 25%  $\text{SiO}_2$  composites [Fig. 8(a,b)]. Therefore, the scattering profiles and SEM data suggest that the  $V(D)$  profiles of these composites are broader

and shifted to larger diameters (maximum at  $\approx 56$  nm) due to local agglomeration effects. In general, these data characterize the gradual change in nanoparticle microstructure from individual particles and aggregates dispersed within a matrix phase to a nearly close-packed arrangement of particles enveloped by the polymer matrix wherein individual aggregates are no longer detectable. The accuracy of the log-normal volume fraction size distribution model was verified by calculating the total component volume fractions,  $\Phi_T$ , for all the composites using the scattering invariant method, as described previously.

### Effect of silane composition on composite morphology

The dispersion state of silica nanoparticles in a polymerized matrix is of practical importance in the field of polymeric dental restorative materials because nanoparticle fillers are being used increasingly in microfilled and hybrid composites. Nanoparticle dispersion quality will ultimately affect the properties of these materials. Both particle-particle and particle-matrix interactions influence particle dispersion quality and the chemistry of the silane agent on the surface of the silica plays a major role in determining the nature of these interactions.

To study the effect of silane interphase composition on nanoparticle dispersion quality, the combined SANS/USANS data were fit using models that assume at least two size distributions are present. The first distribution models the individual silica particles and includes interference effects between particles. The other distributions model the particle aggregates and were tailored to accommodate the fitting curve. For the 10 and 25%  $\text{SiO}_2$  composite scattering data, very good fits were obtained using these models. The model fits provide results for the mean nearest-neighbor distance ( $D_{\text{int}}$ ) between the primary particles. As the silane composition changes from 1.0 M to 1.0 O,  $D_{\text{int}}$  decreases from 87 to 78 nm (Fig. 10), suggesting that particles with higher OTMS fractions at the interphase are closer together. At lower silica concentrations (10 and 25%  $\text{SiO}_2$ ), the MPTMS interphase keeps the individual silica nanoparticles better dispersed, on average, than does OTMS. The dual silanized particle distances are intermediate between those of MPTMS and OTMS.

In particle-filled composites, the interplay of particle-matrix interactions and particle-particle interactions, and the relative strengths of these forces, govern the degree of nanoparticle aggregation.<sup>21</sup> In general, when nanoparticles are dispersed in a polymerizing medium, the particles tend to aggregate as the polymer molecular weight increases. It is entropically unfavorable for the growing polymer to be confined between

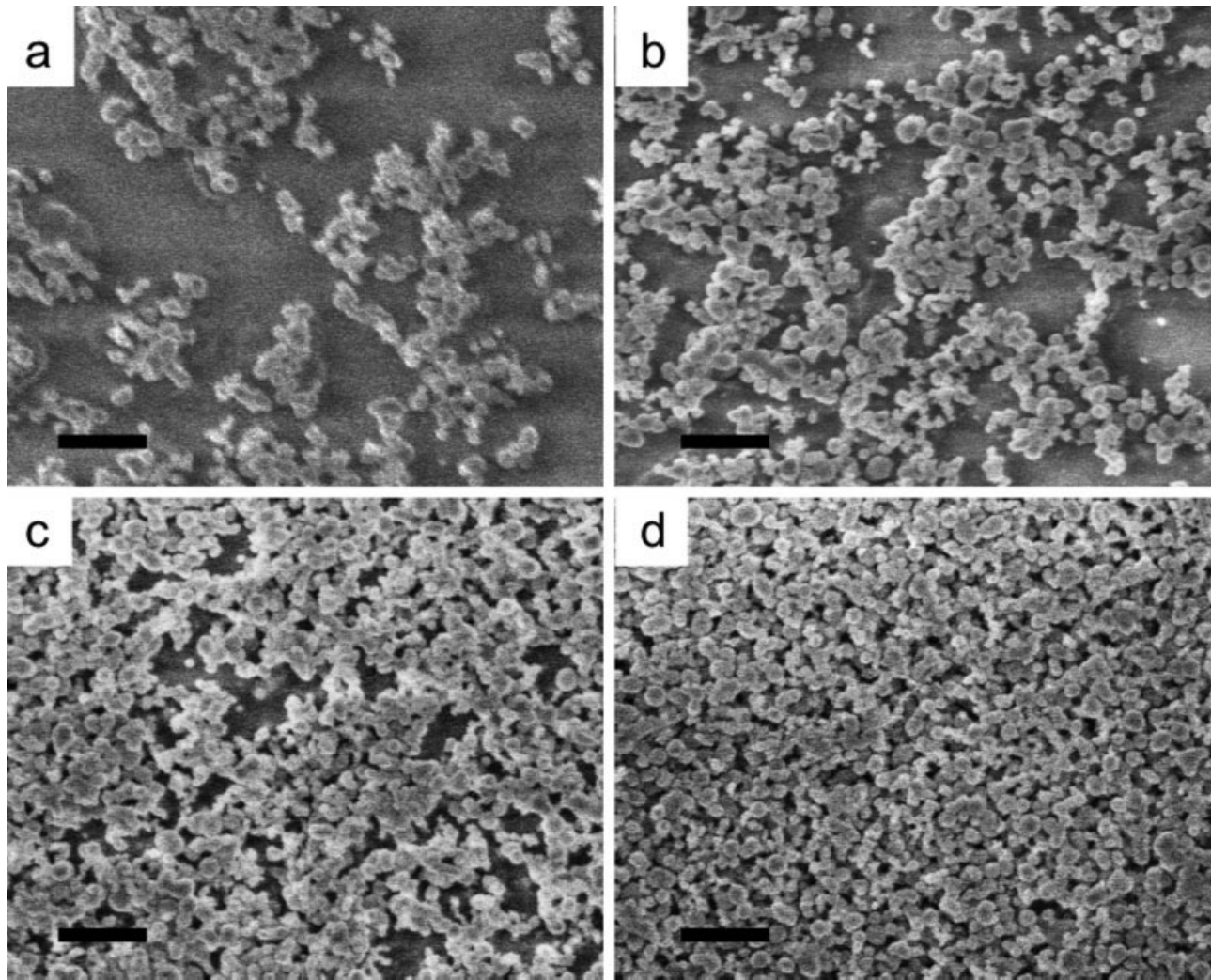


**Figure 8.** Scanning electron micrographs of cut, polished, and oxygen plasma-etched surfaces of (a) 10% (b) 25% (c) 45% and (d) 60% SiO<sub>2</sub> composites. The scale bars equal 500 nm.

the surfaces of particles because of the loss of polymer configurational entropy.<sup>22</sup> The data in this study suggest that in the 10 and 25% SiO<sub>2</sub> composites, the MPTMS-rich interphase overcomes these entropic effects by confining the polymer network between the particles either through H-bonding, covalent bonding, or a combination of both mechanisms. Silica particles coated with OTMS do not bond with the matrix and have enough mobility to move around during polymerization in response to depletion effects.<sup>23</sup>

More evidence that the interphase composition influences nanoparticle dispersion quality is shown in Figure 11 where an increase in aggregate size (second size distribution from the fitting model) is seen for the composite with the OTMS interphase. The model fitting also shows a general trend towards a higher aggregate volume fraction as the fraction of OTMS is increased. All these data suggest that, for the 10 and 25% SiO<sub>2</sub> composites, better dispersion quality is obtained when the interphases

contain MPTMS. Interphases containing only OTMS (1.0 O) produce composites with larger, more compact, aggregates than interphases containing MPTMS.

In the 45 and 60% SiO<sub>2</sub> composites, SANS measured no significant difference in morphology as a function of silane composition, and  $\geq 98\%$  of the particle volume detectable by scattering is in the primary particle size distribution. This suggests the particle distributions and morphologies of the composites with different silane compositions are very similar. Interference distances, and aggregate sizes and volumes, calculated by the model indicate only statistical fluctuations in the nanoparticle distribution. Some polymer-rich phases are observed with a range of sizes by SEM in the 45 and 60% SiO<sub>2</sub> composites with all five interphase compositions (Fig. 12). Most likely, the stochastic polymer rich regions were present during mixing of the uncured composite pastes and were set in place during photopolymerization.

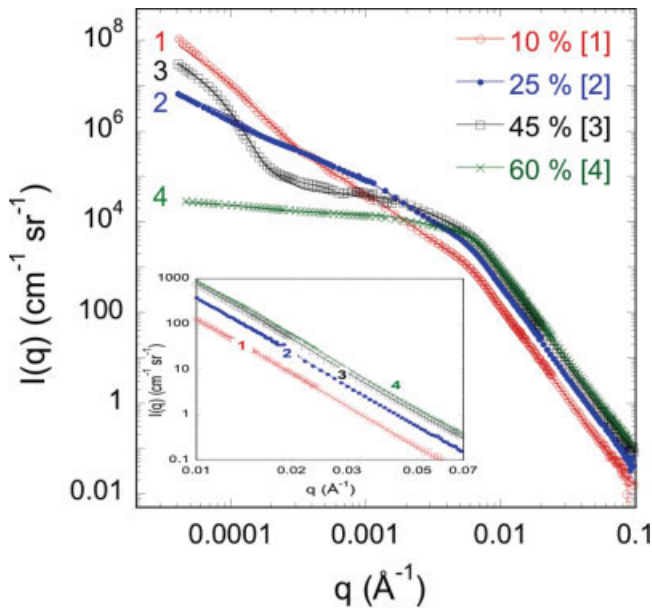


**Figure 9.** Combined data from SANS and USANS for representative 10%, 25%, 45%, and 60% SiO<sub>2</sub> composites containing silica nanoparticles silanized with 1.0 M. The lines are the multi-component lognormal size distribution fits. [Color figure can be viewed in the online issue, which is available at [www.interscience.wiley.com](http://www.interscience.wiley.com).]

**Relationships between interphase composition and composite mechanical properties**

The variations in interphase morphology were measured by small-angle scattering. There is a clear distinction between the three composites with smooth

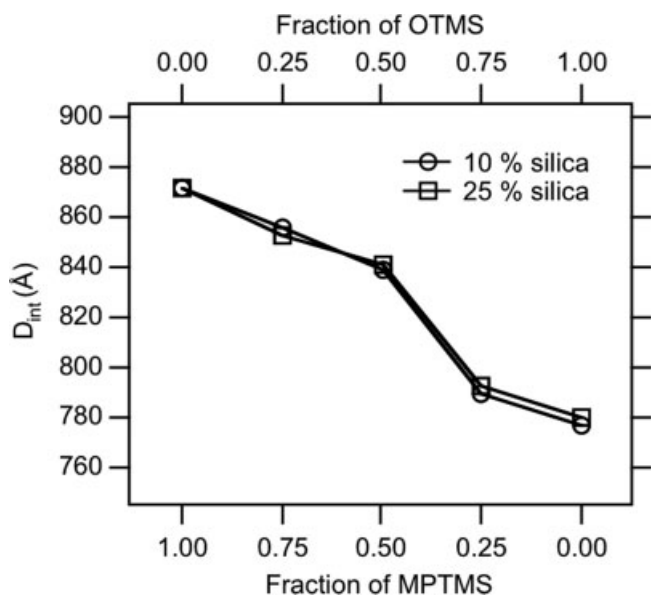


**Figure 10.** Interference distances as a function of silane composition calculated from the model fit data for 10 and 25% SiO<sub>2</sub> composites (Fit uncertainties: ± 15 Å).

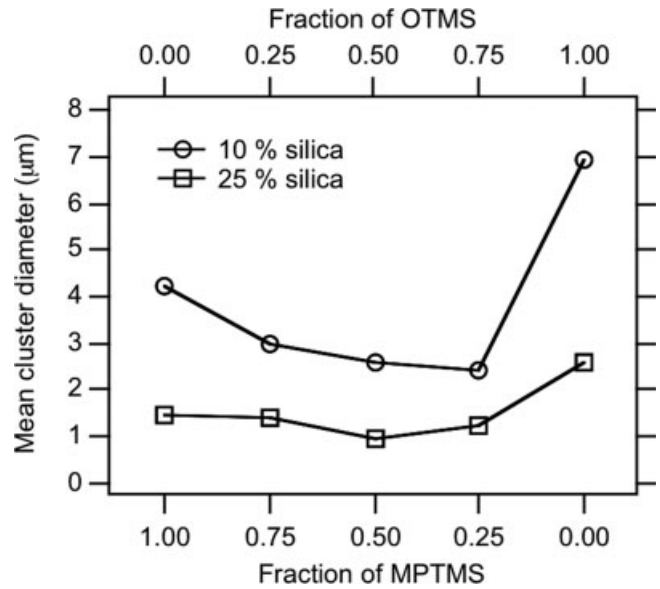


**Figure 11.** Mean cluster diameters (mean diameters of the second size distribution) as a function of silane composition calculated by the model fit for 10 and 25% SiO<sub>2</sub> composites. Lines are drawn to guide the eye.

interfaces (1.0 M, 0.75 M: 0.25 O, and 0.5 M: 0.5 O) and those containing rough, fractal-like interfaces (0.25 M: 0.75 O and 1.0 O). The smooth interface is attributed to the silica nanoparticle/silane network interface and the rough interface is attributed to the OTMS/matrix boundary. The discrete change from smooth to rough interfaces is consistent with the distinct decrease in the composite mechanical properties that occurs for the OTMS-rich composites and is equated with a change from an adhesive to a non-adhesive interphase. The difference between the adhesive and non-adhesive interphases is supported by

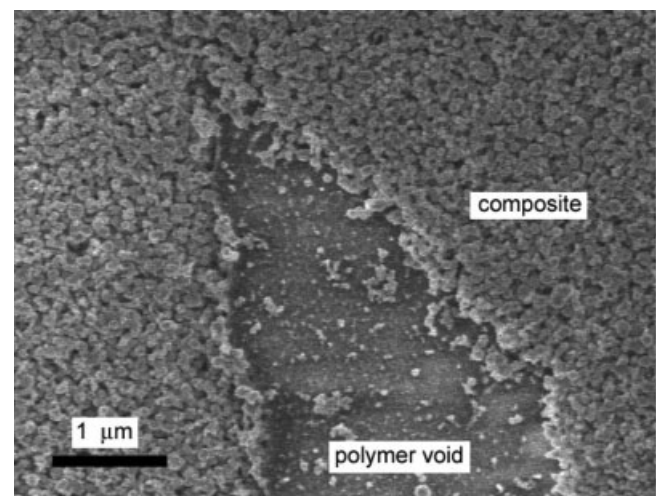


**Figure 12.** Scanning electron micrograph of a 60% SiO<sub>2</sub> composite with a 1.0 O interphase. The stochastic polymer “voids” were distinct from the surrounding composite.

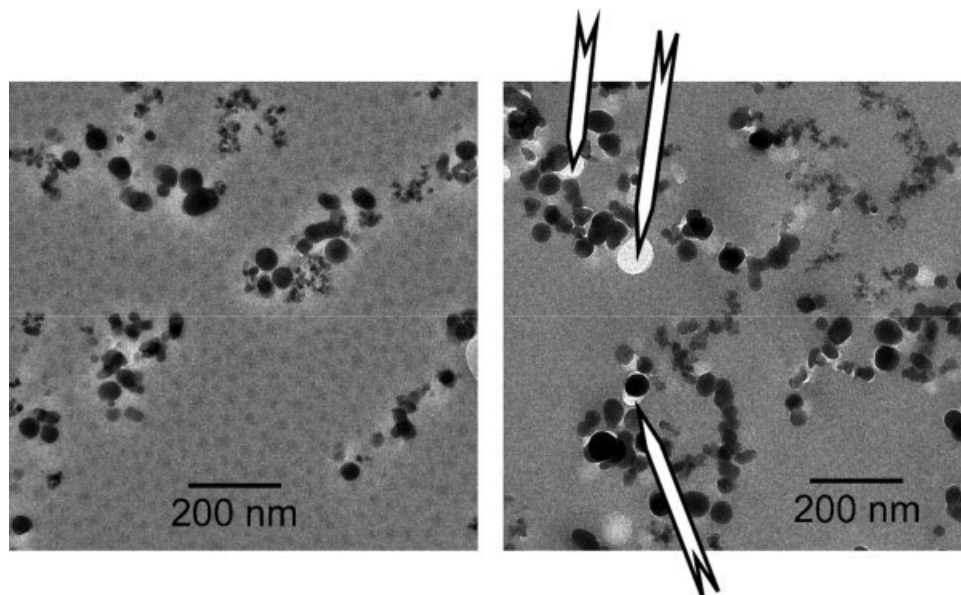


**Figure 13.** TEM images of 10% SiO<sub>2</sub> composites with 1.0 M (left) and 1.0 O (right) interphases. Filler particles appear dark as a result of their high density compared to the surrounding matrix. The mottled appearance of the matrix phase of the 1.0 M composite (left) is an artifact caused by electron irradiation. Arrows (right) indicate regions of poor adhesion and dislodged particles.

TEM images of 10% SiO<sub>2</sub> composites (Fig. 13). All the MPTMS-silanized particles are situated securely in the matrix whereas some of the OTMS-silanized particles are completely dislodged or noticeably disconnected from the matrix, a situation that presumably occurred when the samples were microtomed. In summary, it may be inferred from the 10 and 25% SiO<sub>2</sub> composite data that the 1.0 M, 0.75 M: 0.25 O, and 0.5 M: 0.5 O nanoparticles are better dispersed in the 60% SiO<sub>2</sub> composites than the 0.25 M: 0.75 O and 1.0 O nanoparticles. However, the enhanced mechanical properties of the composites containing MPTMS-rich interphases are primarily attributed to the improved interfacial adhesion between the filler and the polymer matrix mediated by covalent and non-covalent interactions. The slight increase in the BFS of the composite with the 0.5 M: 0.5 O interphase may be attributed to improved mechanical stress relaxation and load transfer at the interface.

## CONCLUSIONS

SANS is an effective method to investigate the morphology of silica nanoparticle dispersions in polymer matrices.<sup>23,24</sup> In our study, the combined SANS and USANS took the scattering measurements to lower  $q$  and larger size than any previous measurements on dental nanocomposites. USANS determined that very large aggregates are not present, which could not have been established using SANS alone.

Under the processing conditions used in this study, the nanoparticle microstructures are relatively consistent among the different interphases. No microstructural advantage or disadvantage was observed with the dual MPTMS/OTMS interphases compared to the 1.0 M interphases for the 60% SiO<sub>2</sub> composites. However,  $D_{\text{int}}$  values and mean cluster diameters calculated for the 10 and 25% SiO<sub>2</sub> composites suggest that the nanoparticles treated with higher mass fractions of MPTMS relative to OTMS are slightly better dispersed than the 1.0 O nanoparticles. The SANS data suggest that the 1.0 M, 0.75 M: 0.25 O and 0.5 M: 0.5 O interphases adhere well to the polymer matrix while the 0.25 M: 0.75 O and 1.0 O interphases are relatively non-adhesive and form a fractally rough interface with the polymer matrix.

The optimal interphase composition is the dental nanocomposite system with the dual 0.5 M: 0.5 O silane blend. Although this silane system contains a high level of the non-bonding OTMS, a strongly adhesive interface results, yielding a composite with enhanced strength and modulus.

A postdoctoral fellowship (K.S.W.) from the National Research Council is greatly appreciated. The authors thank Esstech for their donation of resins and Degussa for their donation of silica. Thanks to the NIST MSEL Microscope Facility for the use of their FE-SEM. The authors thank John Barker both for scientific/technical support for the USANS measurements and for valuable advice regarding the SANS/USANS data interpretation. Finally, the authors

are grateful to Drs. E. Amis, L. Henderson, C. Snyder, S. Hudson, J. Stephens, and B. Vogel of the NIST Polymers Division and S. Claggett of the NIST Metallurgy Division for technical guidance and assistance.

## References

- Antonucci JM, Stansbury JW. Molecularly designed dental polymers. In: Arshady R, editor. *Desk Reference of Functional Polymers*. Washington, DC: American Chemical Society; 1997. pp 719–738.
- Moszner N, Salz U. New developments of polymeric dental composites. *Prog Polym Sci* 2001;26:535–576.
- Kalachandra S, Sankarapandian M, Shobha HK, Taylor DF, McGrath JE. Influence of hydrogen bonding on properties of Bis-GMA analogues. *J Mater Sci Mater Med* 1997;8:283–286.
- Sideridou I, Tserki V, Papanastasiou G. Study of water sorption, solubility and modulus of elasticity of light-cured dimethacrylate-based dental resins. *Biomaterials* 2003;24:655–665.
- Halvorson RH, Erickson RL, Davidson CL. The effect of filler and silane content on conversion of resin-based composite. *Dent Mater* 2003;19:327–333.
- Xu HHK, Quinn JB, Smith DT, Antonucci JM, Schumacher GE, Eichmiller FC. Dental resin composites containing silica-fused whiskers: Effects of whisker-to-silica ratio of fracture toughness and indentation properties. *Biomaterials* 2002;23:735–742.
- Ferracane JL. New polymer resins for dental restoratives. *Oper Dent Suppl* 2001;6:199–209.
- Lalatonne Y, Richardi J, Pileni MP. Van der Waals versus dipolar forces controlling mesoscopic organizations of magnetic nanocrystals. *Nat Mater* 2004;3:121–125.
- Wilson KS, Zhang K, Antonucci JM. Systematic variation of interfacial phase reactivity in dental nanocomposites. *Biomaterials* 2005;26:5095–5103.
- Condon JR, Ferracane JL. Reduced polymerization stress through non-bonded nanofiller particles. *Biomaterials* 2002;23:3807–3815.
- Anusavice KJ. *Phillips' Science of Dental Materials*. Philadelphia: WB Saunders; 1996.
- O'Brien WJ. *Dental Materials and Their Selection*. Chicago: Quintessence Publishing; 1997.
- Biosvert JP, Persello J, Guyard A. Influence of the surface chemistry on the structural and mechanical properties of silica-polymer composites. *J Polym Sci Part B: Polym Phys* 2003;41:3127–3138.
- Chen TM, Brauer GM. Solvent effects on bonding organo-silane to silica surfaces. *J Dent Res* 1982;61:1439–1443.
- Xu HHK, Smith DT, Schumacher GE, Eichmiller FC, Antonucci JM. Indentation modulus and hardness of whisker-reinforced heat-cured dental resin composites. *Dent Mater* 2000;16:248–254.
- Glinka CJ, Barker JG, Hammouda B, Krueger S, Moyer J, Orts W. The 30m SANS instruments at NIST. *J Appl Cryst* 1998;31:430–445.
- Drews AR, Barker JG, Glinka CJ, Agamalian M. Development of a thermal-neutron double-crystal diffractometer for USANS at NIST. *Phys B: Condens Matter* 1997;240:189–191.
- Porod G. General theory. In: Glatter O, Kratky O, editors. *Small-Angle X-ray Scattering*. London: Academic Press; 1982. pp 17–51.
- Schmidt PW. Small-angle scattering studies of disordered, porous, and fractal systems. *J Appl Cryst* 1991;24:414–435.
- Allen AJ, Krueger S, Skandan G, Long GG, Hahn H, Kerch HM, Parker JC, Ali MN. Microstructural evolution during the sintering of nanostructured ceramic oxides. *J Am Ceram Soc* 1996;79:1201–1212.
- Vrij A. Polymers at interfaces and the interactions in colloidal dispersions. *Pure Appl Chem* 1976;48:471–483.
- Henderson D, Kovalenko A, Pizio O, Wasan D. The effective interaction between colloidal hard sphere particles in a polymerizing solvent. Application of Wertheim's theory of association. *Phys A: Stat Mech Appl* 1997;245:276–296.
- Berriot J, Montes H, Martin F, Mauger M, Pyckhout-Hintzen W, Meier G, Frielinghaus H. Reinforcement of model filled elastomers: Synthesis and characterization of the dispersion state by SANS measurements. *Polymer* 2003;44:4909–4919.
- Becker C, Kutsch B, Krug H, Kaddami H. SAXS and TEM investigations on thermoplastic nanocomposites containing functionalized silica nanoparticles. *J Sol-Gel Sci Technol* 1998;13:499–502.